

# Testing the Palma-Clary Reduced Dimensionality Model Using Classical

## Mechanics on the $\text{CH}_4 + \text{H} \rightarrow \text{CH}_3 + \text{H}_2$ Reaction

*Anna Vikár, Tibor Nagy and György Lendvay\**

### AUTHOR INFORMATION

#### **Corresponding Author**

\*G. Lendvay. E-mail: [lendvay.gyorgy@ttk.mta.hu](mailto:lendvay.gyorgy@ttk.mta.hu), Telephone: 00363826508

Institute of Materials and Environmental Chemistry, Research Centre for Natural Sciences, Hungarian  
Academy of Sciences, Magyar tudósok körútja 2. H-1117 Budapest, Hungary

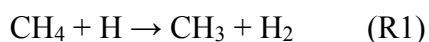
**KEYWORDS** Reduced dimensionality quantum scattering, Palma-Clary Hamiltonian, reaction cross section, quasiclassical trajectory method, one-period averaging method.

**ABSTRACT** Application of exact quantum scattering methods in theoretical reaction dynamics of bimolecular reactions is limited by the complexity of the equations of nuclear motion to be solved. Simplification is often achieved by reducing the number of degrees of freedom to be explicitly handled by freezing the less important spectator ones. The reaction cross sections obtained in reduced-dimensionality (RD) quantum scattering methods can be used in the calculation of rate coefficients, but their physical meaning is limited. The accurate test of the performance of a reduced-dimensionality method would be a comparison of the RD cross sections with those obtained in accurate full-dimensional (FD) calculations, which is not feasible due to the lack of complete full-dimensional results. However, classical mechanics allows one to perform reaction dynamics calculations using both the RD and the FD model. In this paper an RD vs. FD comparison is made for the 8-dimensional Palma-Clary model on the example of four isotopologs of the  $\text{CH}_4 + \text{H} \rightarrow \text{CH}_3 + \text{H}_2$  reaction, which has 12 internal dimensions. In the Palma-Clary model the only restriction is that the methyl group is confined to maintain  $C_{3v}$  symmetry. Both RD and FD

opacity and excitation functions as well as differential cross sections were calculated using the quasiclassical trajectory method. The initial reactant separation has been handled according to our one-period averaging, 1PA method [Nagy, T.; Vikár, A.; Lendvay, G. *J. Chem. Phys.* **2016**, *144*, 014104]. The RD and FD excitation functions were found to be close to each other for some isotopologs but in general, the RD reactivity parameters are lower than the FD ones beyond statistical error and for one of the isotopologs the deviation is significant. This indicates that the goodness of RD cross sections cannot be taken for granted.

## 1. INTRODUCTION

In theoretical chemical reaction dynamics, atomic and molecular encounters are described at the atomic level. In systems where the Born-Oppenheimer approximation is valid, the motion of atoms represented by their nuclei can be handled separately from that of the electrons, and the forces acting on the nuclei are provided by the solution of the electronic Schrödinger equation at the given nuclear configuration. Atoms are microscopic particles so that the accurate way of describing nuclear motion is the solution of the respective Schrödinger equation. In collisional dynamics this means that the solutions corresponding to the continuum of the spectrum of the Hamiltonian operator need to be found. Because of this, development of universal procedures such as those working very well in electronic structure theory is not straightforward. Instead, every class of reaction needs to be handled individually. The number of degrees of freedom to be treated for an  $N$ -atomic system is  $3N-6$  (or  $3N-5$ ), which limits the complexity of the reactions that can be described by accurate quantum scattering techniques. Currently triatomic systems can be handled routinely<sup>1</sup> even when the reactants form a long-lived complex.<sup>2,3,4</sup> There are techniques that allow complete description of four-atomic systems<sup>5,6,7</sup>. The most complex system for which fully quantum mechanical state-to-state reaction probabilities have been obtained so far is the six-atomic



reaction,<sup>8,9,10</sup> but even there the total angular momentum is restricted to 0.

Because of the complexity of quantum scattering calculations, the early reactive scattering methods introduced simplifying assumptions. Triatomic atom-transfer reactions were first treated by confining the motion of atoms along a straight line.<sup>11,12,13</sup> This way the number of degrees of freedom to be handled

explicitly has been reduced to 2. The model not only disregarded the rotation of the diatomic molecule but also the total rotation of the system was also frozen. The latter constraint has been released in the Rotating Linear Model (RLM).<sup>14,15,16</sup> The models were further refined by introducing the Bending Corrected Rotating Linear Model (BCRLM) by several groups<sup>17,18</sup> almost simultaneously which allowed the rotation of the diatomic molecule to be treated via an adiabatic bending potential. The models were extended to four-atomic reactions by Clary and coworkers<sup>19,20,21</sup> by replacing one of the three atoms by a diatomic molecule and allowing it to rotate (Rotating Bond Approximation) as well as by Bowman and coworkers,<sup>18,22,23</sup> who introduced a family of versions of the Collinear Exact Quantum (CEQ) model whose complexity increases systematically as well as the J-shifting and bend energy-shift approximations. For molecules involving more than four atoms, Clary and Nyman<sup>24,25</sup> first applied the RBA method to the reaction  $\text{CH}_4 + \text{OH} \rightarrow \text{CH}_3 + \text{H}_2\text{O}$ . Yu and Nyman included the umbrella bending mode with the Rotating Linear Umbrella model<sup>26,27,28</sup> which is devoted to describe reactions of an atom with a tetrahedral molecule such as reaction (R1), confining the attacking atom, the abstracted (generally H) and the central (carbon) atom along a straight line. The model was extended to handle the bending of the methyl group out of the line of the active modes (Rotating Bond Umbrella model).<sup>29,30</sup> In another line of development J.Z.H. Zhang introduced the Semirigid Vibrating Rotor Target (SVRT) method<sup>31,32</sup> for calculations on atom-polyatomic molecule reactions, which was extensively used for four-atomic systems<sup>33</sup>. This method has been applied to a 4-dimensional quantum scattering calculation similar to the RBU model on reaction R1 in which the methane molecule kept  $C_{3v}$  geometry, the spectator C–H bond length was fixed at the saddle point value.<sup>34,35</sup> Wang and Bowman<sup>36</sup> performed a 6D calculation for reaction R1 treating it as an atom+triatomic molecule system with the three atoms being treated as a pseudo-atom. The method that includes the most degrees of freedom explicitly in a quantum scattering calculation is based on the Palma-Clary Hamiltonian<sup>37,38,39</sup>. This model is designed to describe  $\text{CZ}_3\text{Y} + \text{X} \rightarrow \text{CZ}_3 + \text{YX}$  type reactions by constraining the  $\text{CZ}_3$  moiety to  $C_{3v}$  symmetry, because of which the three C-Z bonds are virtually unbreakable as all of them should be broken simultaneously, and only the fourth atom (Y) can be abstracted or substituted by the attacking X atom. Due to the constraints, the number of internal degrees of freedom to be treated explicitly is reduced to 8. However, including the total angular momentum into the Hamiltonian, in fact 11 degrees of freedom have been handled out of 15 dimensions of

the full-dimensional system when the translation of the center of mass is disregarded. The model has been extensively applied by the group of D. H. Zhang<sup>40,41,42,43</sup> and more recently of M. H. Zhang.<sup>44,45</sup>

In all such approximate models, some selected active degrees of freedom are treated explicitly, while the rest are considered spectators and do not enter the equations of motion. Instead, they are either considered frozen at their equilibrium value or are introduced into the model via the potential energy term by averaging over their vibrations their influence on the active degrees of freedom<sup>46</sup>. Bowman coined the term “reduced dimensionality methods” (RD from now on) to refer to approximate quantum mechanical models of this kind as compared with the complete, full-dimensional (FD) model. The RD techniques, in fact, can be seamlessly utilized in the calculation of rate coefficients. An excellent exposition has been given by Bowman and Wagner<sup>47</sup>. The basic idea<sup>48</sup> is that in the rate coefficient formula of transition state theory (TST), one replaces some contributions to the partition function by parameters obtained from dynamics. In other words, the dynamical information obtained about the active degrees of freedom in RD calculations is supplemented by a statistical treatment of the spectator modes. In the calculations by the Clary group, the method has been extended to variational TST and has been extensively used.<sup>46,49,50</sup> Because the cross sections obtained in RD calculations are valid in a constrained world, they, strictly speaking, have no direct physical meaning.

In some recent papers, however, RD quantum mechanical cross sections have been used to get some information about the real or full-dimensional dynamical behavior of a system. For example, Clary and Meijer<sup>51</sup> used a method called torsional close coupling – infinite order sudden approximation to calculate how a collision by a rare gas atom can excite the hindered rotation of a peptide chain around different bond. The limits of adequacy of such calculations are obvious, as the authors emphasize. Recently, the reaction cross sections obtained with the Palma-Clary Hamiltonian have been directly compared with experimental data. More precisely, Zhang and coworkers<sup>52</sup> calculated the excitation function for the  $\text{CD}_4 + \text{H} \rightarrow \text{CD}_3 + \text{DH}$  reaction and found that its shape is similar to those obtained in the experimental *relative* reaction cross sections by Yang and coworkers. Since the latter were relative, they were made absolute by scaling them to the RD quantum mechanical cross sections at a single point.

Reducing the number of dimensions with respect to the correct FD model is an approximation. However, it is not easy to judge what is lost with respect to reality when dimension reduction is introduced. The ultimate test of the goodness of reduced-dimensionality quantum scattering models would be a comparison of RD cross sections with those obtained in an exact full-dimensional calculation. This is not feasible except for the specific case of the  $\text{CH}_4 + \text{H}$  reaction for which Manthe *et al.* calculated FD state-to-state reaction probabilities, but the comparison of these with the RD results was restricted to zero total angular momentum<sup>8-10</sup>. Classical mechanics, however, offers a possibility to test what dynamical information is lost in RD model calculations, since classically full-dimensional calculations are also feasible. The practice of reaction dynamics shows that, apart from quantum effects that are manifested under some conditions, classical mechanics describe well the basic qualitative features of atomic motion in chemical reactions. Accordingly, if one derives the classical mechanical analog of a RD quantum dynamics method, and performs calculations both with the RD and FD model, the comparison can tell, at least semiquantitatively, the possible deficiencies of the RD model.

Our purpose in this work is to make such comparisons for the Palma-Clary model. We chose reaction R1 and three of its isotopic variants for the test and used two different potential energy surfaces (PES), the CBE PES of Corchado *et al.*<sup>53</sup> as well as the ZBB3 PES by Zhang *et al.*<sup>54</sup> In this work, we concentrate on the dynamical parameters characterizing the reaction, and compare reaction probabilities, excitation functions and differential cross sections calculated with the Palma-Clary (hereafter referred to as RD) and the FD model using the quasiclassical trajectory method. We derived the classical Hamiltonian equations of motion corresponding to the Palma-Clary model. However, we encountered a number of numerical difficulties with trajectory integration, and found that the most productive way to avoid them is that one performs the integration in Cartesian coordinates, enforcing the constraints characterizing the model by the introduction of constraint forces as described by Raff and Thompson.<sup>55</sup> During the calculations we encountered an additional complication: as shown earlier,<sup>56</sup> in our system the normal mode sampling method used for generating initial conditions in the FD model proved to produce nonstationary ensembles and the reactivity parameters were found to periodically oscillate as a function of the initial distance between the reactants. The reason for the oscillations was found to be the periodic variation in the ensemble average value of the

physical parameter (the C-H bond length) to that the reaction was directly sensitive. We have shown that the way to obtain physically meaningful reaction probabilities and cross sections can be generated by averaging over a full oscillation period. We found that the same problem arises in the RD calculations and made sure that the right reactivity parameters were used in the comparison (see in the Methods section).

In this paper we first give a brief overview of the technical details, followed by the comparison of RD and FD reaction probabilities, excitation functions and product angular distributions. In the final section we discuss various dynamical observations that the investigation of the classical RD and FD models provide on the performance of the Palma-Clary model.

## 2. METHODS

**2.A. Generation of ensembles of initial states of CZ<sub>3</sub>Y.** Normal mode sampling was used to sample rovibrational ground-state ensembles of methane molecules to provide initial conditions for the QCT calculations. For the normal mode analysis, in the case of the full-dimensional calculations Cartesian coordinates were used, while for the 5D methane of the Palma-Clary model we used rectilinear internal coordinates shown in Figure 1:  $l$  is the distance of the vertices of the  $Z^1Z^2Z^3$  regular triangle from its geometrical center, denoted as  $Z_3$ , and  $s$  is the distance between the C atom and  $Z_3$ . In addition, we defined a Cartesian frame fixed to CZ<sub>3</sub>: its origin lies at C, its  $z$  axis coincides with 3-fold symmetry axis of CZ<sub>3</sub> (with  $(\mathbf{r}_{Z2}-\mathbf{r}_{Z1}) \times (\mathbf{r}_{Z3}-\mathbf{r}_{Z1})$  defining the positive  $z$  direction) and the  $x$ - $z$  plane contains  $Z^1$ . The position of the Y atom is given by 3 Cartesian coordinates  $(x_Y, y_Y, z_Y)$  in this frame.

In the FD model of methane, normal mode sampling was carried out following the standard procedures<sup>57</sup> as has been described in detail in Ref. 56. In the reduced-dimensional model, normal mode sampling was carried out based on the pure vibrational Hamiltonian expressed in the reduced set of internal coordinates, whose derivation follows line of thoughts similar to those in sections II.A and II.B.1 in Ref. 58, except that the pure vibrational Hamiltonian of internal coordinates was constructed. The applied methodology is completely general as it requires only the transformation equations from the internal to body-fixed Cartesian coordinates. With this Hamiltonian, the standard formal procedure of normal mode analysis and sampling

was followed to generate ensembles of semiclassically quantized classical states of CH<sub>4</sub> molecules, which were then randomly oriented using Euler rotations.

In the following, atomic units are used,  $a_0=0.529$  Å for distance,  $\tau_0=2.419\times 10^{-17}$  s for time and occasionally  $E_h=27.21$  eV for energy.

The normal mode sampling method has earlier been found to produce nonstationary ensembles of classical states<sup>56</sup> for the methane molecules on both the CBE and ZBB3 PESs. As a consequence, the calculated reactivity parameters depend on the time the reactants spend from the beginning of the integration of the trajectory until they arrive in the strong interaction zone in a trajectory. The duration of the free flight is determined by the initial separation of the reactants, and the time development of the ensemble representing the initial quantum state is mapped into a distance dependence of the reactivity parameters. This is what has been seen in full-dimensional QCT calculations<sup>56</sup> on reaction R1 and its isotopic variants. The evolution of the ensembles of initial states of reactants produced a periodic oscillation of the ensemble average of the C–H bond length with a period ( $T_{osc}$ ), and this appeared as an oscillation of the calculated reaction probabilities and cross sections as a function of the initial distance between the reactants, causing a significant uncertainty in their determination. In the reduced dimensionality calculations presented in this paper, the same behavior has been observed. Such dependence makes the physical meaning of the calculated parameters questionable. In this work we eliminated the uncertainty caused by the reactivity oscillation using the one-period averaging (1PA) method proposed earlier,<sup>56</sup> according to which the reactivity parameters are averaged over a time segment covering a full oscillation period. In practice,  $T_{osc}$  was determined in preliminary calculations. It proved to be equal to the period of the corresponding stretch vibration (symmetric stretch for the CZ<sub>4</sub> and the local stretch for the CZ<sub>3</sub>Y isotopologs), about  $T_{osc}=460 \tau_0$  for C–H and  $T_{osc}=620 \tau_0$  for C–D bonds (see also Ref. 56). Averaging was performed in the following way: after the standard preparation, each classical state in the initial ensemble of methane molecules was propagated for a random time uniformly sampled from the interval  $[0, T_{osc}]$  and the collisions were initiated from the obtained states.

Random numbers were generated with a Marsaglia-Zaman algorithm<sup>59</sup> using the randgen.f code available online.<sup>60</sup>

**2.B. Quasiclassical trajectory calculations.** The CZ<sub>3</sub>Y + X collisions were simulated by integrating

Hamilton's equations of motion using 18 lab-frame Cartesian coordinates and momenta for both the FD and the RD model. In the reduced-dimensionality model the constraints (1)-(4),

$$f_1(\mathbf{x}_{3N}) = \mathbf{r}_{CZ1}^2 - \mathbf{r}_{CZ2}^2 = 0 \quad (1)$$

$$f_2(\mathbf{x}_{3N}) = \mathbf{r}_{CZ2}^2 - \mathbf{r}_{CZ3}^2 = 0 \quad (2)$$

$$f_3(\mathbf{x}_{3N}) = \mathbf{r}_{CZ1} \mathbf{r}_{CZ2} - \mathbf{r}_{CZ2} \mathbf{r}_{CZ3} = 0 \quad (3)$$

$$f_4(\mathbf{x}_{3N}) = \mathbf{r}_{CZ2} \mathbf{r}_{CZ3} - \mathbf{r}_{CZ3} \mathbf{r}_{CZ1} = 0 \quad (4)$$

were enforced by calculating the constraint forces using the Lagrange multiplier method<sup>55</sup>. Here,  $\mathbf{r}_{AB}$  denotes the vector between atoms A and B, and  $Z^1$  and  $Z^2$  and  $Z^3$  are the Z atoms in  $CZ_3$ . Constraints (1)-(2) and (3)-(4) guarantee the equality of the three bond lengths and the three ZCZ angles, respectively. The constraint forces were added to those derived from the potential energy surface in Hamilton's equations for the change of momenta. The equations of motion were integrated using the Runge-Kutta method. The step size was  $5 \tau_0 \approx 1.2 \times 10^{-16}$  s to guarantee energy conservation within  $0.05 mE_h$  throughout each trajectory.

Ensembles of classical states of methane molecules corresponding to rovibrational ground state were prepared using normal mode sampling as described above. The number of initial states at each collision energy was  $4 \times 10^5$  in both the RD and the FD calculations. The impact parameter ( $b$ ) was sampled uniformly from the  $[0, 4.75 a_0]$  interval. The initial center of mass distance of the methane molecule and H atom was  $12 a_0$ . Note that the vibrations of the reactant methane had already been integrated for some time before the "collision started" to perform the averaging in the 1PA method (see above). Collision energies ( $E_{\text{coll}}$ ) were scanned between 10 and  $80 mE_h$  in 5 or  $10 mE_h$  steps. The lowest energy is significantly below the classical barrier height of the abstraction reaction (cca.  $24 mE_h$ ,  $0.65 \text{ eV}$ ) because our aim was to compare the full and the reduced dimensional models in the entire reactive range in which quasiclassical trajectory calculations provide reaction. Reactions at energies below the barrier height become possible because of zero-point energy leakage (which does happen in our case, see later). There are several *ad hoc* ways of correcting this problem, none of them being theoretically well founded. The simplest of these is that one neglects trajectories if the internal energy of the post-collision molecules does not exceed their ZPE. However, this procedure treats the products in the FD and RD models differently, so we prefer making the RD/FD comparison of the reactivity parameters in their pristine form, i.e. the trajectories were started from

semiclassically quantized initial conditions but after that no simulation of quantum effects is attempted. All trajectories were handled equally irrespectively whether either of the product molecules or any of their vibrational modes lacked ZPE.

The scattering angle of the diatomic YX product was calculated with reference to the initial velocity vector of the attacking X atom. Product scattering angle resolved reaction probabilities were calculated by binning reactive trajectories according to the cosine of the scattering angle,  $\Theta$  into 0.2 wide bins and carrying out opacity function calculation for each  $\cos\Theta$  bin using 0.5  $a_0$  wide impact parameter bins.

Normal mode analysis, sampling and simulation of trajectories, and the analysis of results were carried out using home-made Fortran codes.

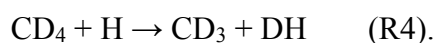
RD and FD reactivity parameters have been evaluated with the QCT method for reaction R1 and for its three isotopic variants in which the  $C_{3v}$  symmetry of the methyl group is meaningful, including the H-atom transfer,



and the D-atom abstractions



and



In the Palma-Clary model only one H or D atom is reactive, while in the FD calculations on reactions R1 and R4 there are four equivalent reactive H and D atoms, respectively. In the FD model of the  $\text{CH}_3\text{D} + \text{H}$  and  $\text{CHD}_3 + \text{H}$  systems the three identical atoms are also reactive but the reaction of the individual atom is distinguished from them. To make RD/FD comparisons more straightforward, we have divided the FD reaction probabilities and cross sections by 4 for reactions R1 and R4, and kept those obtained for reactions R2 and R3 unscaled. To emphasize this, the parameters plotted will be referred to as “per bond” reaction cross sections etc. In the figures the error bars correspond to  $2\sigma$  statistical error.

### 3. RESULTS

**3.A. Vibrational modes and frequencies.** Dimension reduction itself can change the nature and the

frequencies of some normal modes of the reactant methane molecule. Table 1 shows the comparison of the symmetry, degeneracy, type and frequency of the four methane isotopologs on the CBE and ZBB3 PESs. The conclusions drawn below from the data hold for both PESs.

For the  $CZ_4$  isotopologs characterized by  $T_d$  symmetry, both the FD and RD models predict 4 different frequencies. After dimensionality reduction, the symmetric stretch mode remains intact, one of the  $T_2$  stretch modes (the component that keeps the highest symmetry) becomes an asymmetric combination of the C-Y and the C- $Z_3$  stretching (here Y stands for the “reactive” H or D atom of the RD model) and one of the  $T_2$  deformation modes becomes a  $CZ_3$  umbrella vibration. All frequencies remain the same except the one corresponding to the doubly degenerate bend mode that has no direct counterpart in the 5D model.

The symmetry of the  $CZ_3Y$  isotopologs is  $C_{3v}$  already in the FD model, and among the stretch modes one is an essentially local C-H or C-D vibration with a distinctly different frequency, and one is an essentially local  $C_{3v}$  symmetric stretch of the  $CZ_3$ . The reduction of symmetry “generates” the umbrella mode mentioned above. Upon dimension reduction the two local stretch modes remain the same while the doubly degenerate stretch as well as one of the two double degenerate bend modes disappears. Only the fully symmetric modes of the full-dimensional model keep their frequency in the 5D model.

The zero-point energy (ZPE) in the methane molecule decreases due to dimension reduction to about one half, by about 0.56 eV for  $CH_4$  and  $CH_3D$ , and about 0.41 eV for  $CD_3H$  and  $CD_4$ . The energy “lost” from the stretch modes is 0.39 and 0.29 eV in the same order.

**3.B. Reaction probabilities.** Opacity functions ( $P(b)$ ) are shown in Figures 2a-b for both PES at  $E_{\text{coll}} = 50 \text{ m}E_h \approx 1.36 \text{ eV}$ . A characteristic difference can be seen in the shape between the CBE and ZBB3 opacity functions for all isotopologs. On the CBE PES (similarly to the earlier PES by Espinoza-Garcia<sup>61</sup>), the FD opacity functions monotonously decrease from a relatively large value (between 0.5% and 1.4%) at zero impact parameter to zero at about  $4 a_0$ . On the ZBB3 PES the reaction probability at zero impact parameter is significantly lower than on the CBE PES for all reactions. For reactions R1 and R2  $P(b)$  increases to pass a maximum at about 2.2 to 2.7  $a_0$ . For reactions R3 and R4 the reaction probability remains essentially the same in the impact parameters range between 0 and 2.5  $a_0$ . It should be noted that the difference between the

CBE and ZBB3 opacity functions is smaller at lower collision energies and the height of the maximum on the opacity function gradually decreases when  $E_{\text{coll}}$  is reduced. Accordingly, at low collision energies the stripping mechanism is less favored than at high  $E_{\text{coll}}$ .

The opacity functions obtained at 1.36 eV collision energy from the RD model agree within statistical error with those of the FD model in most of the cases (6 out of 8). In the case of reaction R3 on the CBE PES and reaction R4 on the ZBB3, the shapes of the curves are still very similar and the RD opacity functions look like as downscaled versions of the FD ones. The close agreement between the shapes of the RD and FD opacity functions, suggests that the Palma-Clary model can capture the qualitative features of the dynamics of the reactions.

**3.C. Reaction cross sections.** The excitation functions for the two PESs and for the two models are shown in Figures 3a-b for reactions R1-R4. The common features of the FD reaction cross sections ( $\sigma_r$ ) are that they increase first slowly, then fast starting with about 0.2 eV above threshold, and pass a maximum after which the decrease is slower than the initial increase (this latter part is hardly visible for reaction R1 on the CBE PES). For reaction R4 the general shape of the excitation function on the ZBB3 PES agrees well with that obtained by Zhang *et al.*<sup>52</sup> in quantum scattering calculations using a seven-dimensional version of the Palma-Clary Hamiltonian on the ZBB3 PES. The width of the peak in our calculations varies with the isotope combination. On the CBE PES the peaks are much less well defined but the tendencies are similar. The shapes of the RD excitation functions are generally similar to the FD ones. From the FD calculations on the ZBB3 PES, the lowest threshold, below 0.27 eV is observed for reaction R1, the highest, above 0.41 eV for reaction R3, and those for reactions R2 and R4 are between the two. The RD thresholds are higher than the corresponding FD values except for reaction R2 where the two can not be distinguished on the ZBB3 PES.

On the CBE PES for all four reactions and on the ZBB3 PES for three isotopologs, reactions R1, R3 and R4 the RD reaction cross sections are systematically lower than the FD ones. On the CBE PES the RD/FD difference changes moderately with the collision energy except near threshold where the RD cross sections are remarkably smaller than the FD ones except for reaction R2 where they are indistinguishable within statistical error. More diversity can be seen on the ZBB3 PES regarding the magnitude of differences

between the RD and FD model as a function of collision energy. The RD cross section near the threshold for reactions R1, R3 and R4 is significantly lower than the FD one, the RD/FD ratio on both PESs being about 0.5 for CH<sub>4</sub>, below 0.3 for CD<sub>4</sub> and between the two for CH<sub>3</sub>D. The relative magnitude of the difference between the RD and FD cross sections for these reactions decreases fast as the collision energy and the cross sections increase and is the smallest near the maximum of the excitation function on both PESs, but increases again on the high-energy side. The deviation is exceptionally large for reaction R4 on the more realistic ZBB3 PES where at high energies the RD curve falls much faster and the cross sections are below one half of the FD ones.

Reaction R2 represents an exception. On the CBE PES, the FD and RD excitation functions and their differences for this reaction are characterized by parameters similar to those for reaction R1 except that at low collision energies the RD and FD cross sections are very close to each other. In contrast, on the ZBB3 PES the behavior of the cross sections for reaction R2 differ from any of the other seven cases. Here the RD cross sections are within statistical error identical to the FD ones but near the maximum of the curve slightly exceed the latter. This is the only case where the RD cross sections can not be distinguished from the FD ones.

**3.D. Product angular distributions.** The FD and RD angular distributions at 1.36 eV are shown in Figures 4a and 4b for the four reactions on the CBE and ZBB3 PESs, respectively. The FD and RD distributions are qualitatively the same. On the other hand, the angular distributions on the two PESs are drastically different, similarly to what has been found in the comparison of the EG<sup>61</sup> and an on the fly calculated B3LYP/6-31G\* PES.<sup>62,63</sup> The scattering angle resolved reaction probabilities for reaction R1 calculated at  $E_{\text{coll}} = 0.95$  eV (35 mE<sub>h</sub>) on the ZBB3 and CBE PESs are shown in Figure 5. The general behavior for the other isotopologs and at other collision energies is very similar. As expected, the nature of scattering switches from backward ( $\cos\Theta = -1$ ) at low impact parameters toward stripping ( $\cos\Theta = 1$ ) at large ones. Remarkable is the similarity of the RD and FD plots. This indicates that the RD model captures the qualitative features of the dynamics correctly. This is not surprising: the overall shape of the probability distributions in Figure 5 follow the curve obtained for hard-sphere collisions, see Figure 1. in Ref. 64 (note that in that work, the scattering angle of the CD<sub>3</sub> was plotted, not that of HD).

## 4. DISCUSSION

The idea behind reduced-dimensionality models is that for a reaction the dynamics is determined by a few well-selected coordinates and the rest of the degrees of freedom behaves as spectators, i.e. there is little coupling between the two groups of modes. If this condition is not fulfilled and the coupling contributes favorably to reactivity, the reduced-dimensionality model will underestimate reaction cross sections with respect to the full-dimensional, and it will overestimate the cross sections if the coupling frustrates reaction. The results presented in the previous sections show that in general, they are smaller than the FD cross sections, especially in the threshold region. Out of the eight studied cases, there is only one for which the RD excitation function matches that obtained in the FD calculation. In addition to the mere coupling between the active and the spectator modes, there are some other factors that can influence the accuracy of the RD model. In the following we investigate some of these.

An obvious such factor is that, when selecting the important degrees of freedom to be treated explicitly in a RD method, the model may bias the dynamics in favor of reaction. For example, in the rotating linear model designed for triatomic reactions whose saddle point geometry is collinear, one can expect an overestimation of reactivity because it always forces the highly favorable collinear direction of approach and those not appropriate for reaction are neglected. A similar –although much less strong– bias is in the Palma-Clary model the constraint on the symmetry of the  $CZ_3$  group. The saddle point geometry for the H-atom abstraction from methane is of  $C_{3v}$  symmetry. By enforcing the  $CZ_3$  group to retain the same symmetry, one provides a larger chance for the system to pass the barrier region of the PES closer to the saddle point itself, i.e. in the lower energy range, making the RD model more favorable for reaction. The observations presented in Figure 3 show the opposite, i.e. providing an easy channel for the system to go through seems not to help the reaction to come about. This indicates that the FD dynamics probably does involve pathways passing from the reactant to the product arrangement relatively far from the saddle point.

A possible factor inducing larger reactivity in the FD with respect to the RD model can be zero-point energy leakage from the degrees of freedom disregarded in the Palma-Clary model. One can get some information on this by looking into the behavior of the threshold energy for reaction, which is certainly lower when

obtained from QCT calculations than the exact quantum threshold. This indicates that a part of the ZPE is utilized in surpassing the potential barrier. As mentioned in Section 3.C in connection with Figure 3, the threshold energy ( $E_{\text{thr}}$ ) for reactions R1, R3 and R4 is slightly higher on the RD excitation functions than on the FD ones, in other words, in the RD model the threshold is shifted less below the barrier height. This is not surprising considering that there is less ZPE available in the RD model of methane than in the FD one. However, the magnitude of the threshold difference is remarkably smaller than the difference of the ZPEs. When the spectator modes are active (FD model),  $E_{\text{thr}}$  is less than 0.14 eV smaller than when they are switched off (RD model), while the ZPE available for leakage is at least as much as 0.4 eV larger (or 0.3 eV if considering only the stretch modes). This means that in the FD model, not all of the extra ZPE is utilized for the reduction of  $E_{\text{thr}}$ . This is not surprising, and is an indication that the efficiency of the ZPE leakage varies with the type of the “energy-storage” mode and more probably that in the FD model the energy flow from the modes missing from the RD model to the active ones is moderately efficient. This latter observation supports the goodness of the selection of the active and spectator modes in the Palma-Clary model.

Geometrical factors can also be considered when the performance of the RD model is assessed. The shape of the methane molecule can, in principle, provide conditions that are more advantageous in the FD than in the RD model. For example, in the  $\text{CH}_4+\text{H}$  and  $\text{CD}_4+\text{H}$  reactions, in full dimensionality, when the attacking H atom, after missing the chance of reacting with one H or D atom of methane, can meet another one with a new chance for reaction, especially in large-impact parameter glancing collisions. Such effects have been observed and proved to be important in  $\text{H} + \text{O}_2$  and  $\text{O} + \text{O}_2$  collisions.<sup>65,66,67</sup> However, in the RD model, when the only reactive H atom is missed by the attacking H atom, the encounter is unsuccessful from the point of view of reaction, because a possible encounter with a nonreactive H atom is prevented by the repulsive interaction. Among the numerous trajectories we have animated, we have not yet seen such events in reactions (R1) and (R4), but they cannot be excluded. If the “reactivity” of each of the four H atoms in  $\text{CH}_4$  is exactly the same as that obtained in the RD model, then in the full-dimensional calculation the cross sections should be exactly four times larger than the RD ratio. If the scenario of “abstract a second atom after the first was missed” operates, then the effective reactivity will be larger when all four H atoms are

allowed to react than when there is only one and the ratio should be larger than 4. The FD per bond cross sections shown in Figure 3 for reactions (R1) and (R4) are already divided by 4 so they can be directly compared with the RD cross sections. For both reactions on both PESs the FD per bond cross sections are larger than the RD ones. The same relationship can be seen for reaction probabilities in the opacity functions in Figures 2a,b (even though they are laden by larger statistical error), especially where the relative deviation is larger in the large impact parameter range that has a greater weight in determining the cross sections. The fact that the FD/RD reactivity ratio that is larger than unity is consistent with the “attack a second atom after the first was missed” mechanism in reactions R1 and R4. If this mechanism has a non-negligible role in a reaction, then the Palma-Clary model will not be able to take it into account and it can be one factor why the RD per bond cross sections are lower than their FD counterparts.

A special difference in the secondary isotope effect, i.e. the influence of the change of the Z atoms in  $CZ_3Y$  is worth noting. When  $CH_3$  is substituted by  $CD_3$ , the efficiency of H-atom abstraction (reactions R1 and R2) decreases by a factor of roughly 2. In contrast, upon the same substitution, the transfer of a D atom (reactions R3 and R4) speeds up by about a factor of 1.5 or 2 depending on the type of PES. One can see that the abstraction of the Y atom is more efficient when the Z atoms have the same mass as Y. The dynamical reason for this is that when  $Z=Y$ , the stretching modes in which the Y atom participates are all group modes involving also the Z atoms in  $CZ_3$ . The energy transfer between these modes is efficient. In contrast, when  $Z \neq Y$ , the vibrations of Y and of  $CZ_3$  are essentially local due to the significant mass difference between the D and H isotopes, so that there is hardly any coupling between the motion of the reactive Y atom and the  $CZ_3$  vibration. These modes are the same in both the FD and RD models; accordingly, the RD model describes the secondary isotope effect correctly. The enhanced coupling due to mass uniformity is found to be favorable for the reaction. This indicates that the energy transfer from the active modes of the  $CZ_3$  group is essential from the point of view of reaction. (Note that in the quantum world this observation may not be purely manifested, especially in the threshold range because of the tunnel effect.) This coupling is the reason behind the inversion of the secondary isotope effect for H and D-atom transfer, but not necessarily concerns the active-spectator coupling that is the main factor determining the goodness of the Palma-Clary model.

The detailed dynamics of individual collisions can help one to understand the properties why the RD model produces smaller reactivity. We have animated and viewed numerous trajectories for all four isotopologs. Interesting observations were made in animations, in which trajectories were started from the initial conditions generated for the RD model, but the integration was performed either using the RD or the FD trajectory code. (Note that both of them work in 18 Cartesian coordinates and momenta but in the RD calculations the  $CZ_3$  group's  $C_{3v}$  symmetry restrictions are enforced using constraint forces.) Not surprisingly, the RD and FD movies showed very similar scenarios, because during the relatively short flight time the energy deposited into the modes of the FD model did not spread seriously into the other, originally “empty” modes. The reason for this is the relatively small coupling between the modes. A remarkable proof of this has been provided by some trajectories that proved to be reactive in the RD model. Namely, the reactive FD trajectories generally follow the same path as the RD ones even after the atom transfer was essentially complete (the scattering angle, the magnitude of product vibrational and rotational excitation etc. are essentially the same.) In some cases, however, after the product diatomic molecule started to depart during an FD trajectory, a “kick” from some of the atoms of the  $CZ_3$  group forced it to return, re-establishing the original C–Y bond. This kind of dynamics reflects the enhancement of coupling in the FD model between the spectator and active modes in the strong interaction zone where all atoms are close. This kind of active-spectator mode coupling, manifested particularly in the post-barrier region of the PES is a feature the Palma-Clary model may miss.

Finally, it is worth mentioning that the dynamical behavior of the RD and FD models on different potential energy surfaces can provide information on which features of the PESs are responsible for the differences in the dynamical parameters of the same reaction. For example, we have seen that the behavior of the opacity functions and the product angular distributions calculated on the ZBB3 and the CBE PESs differ qualitatively. In the opacity functions (Fig. 2b) the relatively small reaction probability at zero impact parameter and the presence of the maximum obtained on the ZBB3 PES indicates that on this surface, much larger fraction of reactive collisions take place via the stripping mechanism, while on the CBE PES in the majority of reactive collisions the product XY molecule bounces back with respect to the direction of the attack by the atom. This can also be seen in Figure 4: the magnitude of the reaction probability on the large

impact parameters/more forward scattering wing of the scattering angle resolved reaction probability plot is much larger on the ZBB3 PES than on the CBE PES. In the experiments by Zare *et al.*<sup>64,63,64</sup>, for reaction R4 predominantly forward scattered HD molecules have been observed at collision energies in the 1 to 2 eV range. The concomitant QCT simulations showed that the EG PES<sup>61</sup> that is similar to but less accurate than the CBE PES used in the present work, produces results on several parameters such as angular distributions and product energy partitioning that deviate qualitatively from the experimental observations. In contrast, trajectory calculations on the B3LYP/6-31G\* PES obtained on the fly do reproduce the experimental parameters. The difference has been assigned to the shape of the potential energy surface as a function of the C–Y–X angle. Here we can see the same tendencies in the dynamical parameters (opacity function, angular distributions) in connection with the CBE vs. ZBB3 PES comparison. Moreover, the tendencies are the same both in the FD and the RD calculations. This means that the factor inducing the qualitative differences on the CBE vs. ZBB3 PES is among the degrees of freedom that the RD model also treats explicitly, and indicates that in this respect the behavior of the CBE PES is similar to that of the original EG PES. The C–Y–X bending motion is among the modes included in the RD model, so the FD/RD agreement corroborates that the difference in the dynamics can be assigned to the shape of the bending part of the PES.

## 5. CONCLUSIONS

The possibility that in classical mechanics both full-dimensional (FD) and reduced dimensionality (RD) reaction dynamics calculations are feasible has been utilized to assess the properties of the Palma-Clary model that is widely used in quantum scattering calculations. QCT calculations were performed on two potential energy surfaces for the  $\text{CH}_4 + \text{H} \rightarrow \text{CH}_3 + \text{H}_2$  reaction and its three isotopic variants, using normal mode sampling to generate initial conditions for the vibrational ground state of the reactant methane both according to the FD and the RD model. No attempts were made to simulate any quantum effects afterwards, allowing pure classical mechanics to operate during collisions.

The calculated reaction probabilities and cross sections were found to be lower beyond statistical error when calculated with the RD model than with the FD one except in one of the eight PES-isotopolog combinations. The RD reactivity parameters are significantly smaller than the FD ones in the (classical) threshold region. The largest difference has been found for the  $\text{CD}_4 + \text{H} \rightarrow \text{CD}_3 + \text{DH}$  reaction on the

more realistic (ZBB3) of the two investigated PESs. This suggests that the rate coefficients calculated directly (i.e., without any correction to redeem the disregarded dimensions) from the RD excitation functions will be much smaller than those obtained in a real full-dimensional one. We have discussed various factors that may indicate which kind of coupling may be responsible for the deviations. The deviation of the RD excitation functions from the FD ones also hints that one needs to be cautious when comparing experimentally measured cross sections with those from RD quantum scattering calculations, such as done in Ref. 52. Our overall conclusion from the classical mechanics studies is that the reduced-dimensionality model provides results close to the full-dimensional one in some cases while in other cases significant deviations can be seen; the consequences of dimensionality reduction seem hard to predict.

We need to emphasize that the RD QCT calculations and their comparison with the FD ones is not as straightforward as it looks at first sight. First, the normal mode sampling routinely used in QCT calculations on polyatomic molecules turned out to generate nonstationary ensembles of initial states for our molecules, because of which the reaction cross sections oscillate as a function of the initial distance between the reactants (proportional to the initial duration of free flight during which the ensemble of reactant molecules evolves). The uncertainty can be eliminated by averaging over one period of the artificial cross section oscillation (for details see Ref. 56). The proper way of averaging requires preliminary tests both in full and reduced dimension. Another difficulty is the reliable simulation of one of the quantum effects, in particular, ZPE loss. In this paper we do not intend to discuss these questions; it will be the subject of a future paper. It is worth mentioning that, in contrast to quantum scattering calculations, RD QCT calculations are not necessarily significantly less expensive than the full-dimensional ones when the number of degrees of freedom is not much less than in a full-dimensional model. The reason is that when using nonlinear coordinates, calculation of the terms in Hamilton's equations of motion are computation-demanding or, as we have done in this case, the same number of degrees of freedom has to be integrated with the additional task of solving a set of constraint equations at every time step.

## ACKNOWLEDGMENTS

We thank Professors J. Espinosa-Garcia and J. M. Bowman for making the potential surface codes available

for us. This work has been supported by the Hungarian Scientific Research Fund (Grant No. K108966) and by the National Development Agency (Grant No. KTIA\_AIK\_12-1-2012-0014).

## Figure Captions

**Figure 1.** Internal coordinates ( $x_Y, y_Y, z_Y, s, l$ ) of the reduced-dimensional model of methane used for normal mode sampling of initial states. The  $CZ_3$  group is constrained to  $C_{3v}$  symmetry. See details in text.

**Figure 2.** Opacity functions for reactions R1-R4 calculated at collision energy 1.36 eV on the (a) CBE and (b) ZBB3 PESs calculated with the RD and FD models. Per bond reaction probabilities are shown for easier comparison.

**Figure 3.** Excitation functions calculated for reactions R1 – R4 with the RD and FD models on the (a) CBE and (b) ZBB3 PESs. For easier comparison, per bond reaction cross sections are shown.

**Figure 4.** Product angular distributions calculated for reactions R1 – R4 with the RD and FD models on the (a) CBE and (b) ZBB3 PESs at  $E_{\text{coll}} = 1.36$  eV.

**Figure 5.** Scattering angle and impact parameter resolved reaction probabilities for reaction R1 calculated with the RD (a,c) and FD (b,d) models at collision energy 0.95 eV on the CBE (a,b) and ZBB3 (c,d) PESs. Per bond reaction probabilities are shown for easier comparison.

**Figure 1.** Internal coordinates  $(x_Y, y_Y, z_Y, s, l)$  of the reduced-dimensional model of methane used for normal mode sampling of initial states. The  $CZ_3$  group is constrained to  $C_{3v}$  symmetry. See details in text.

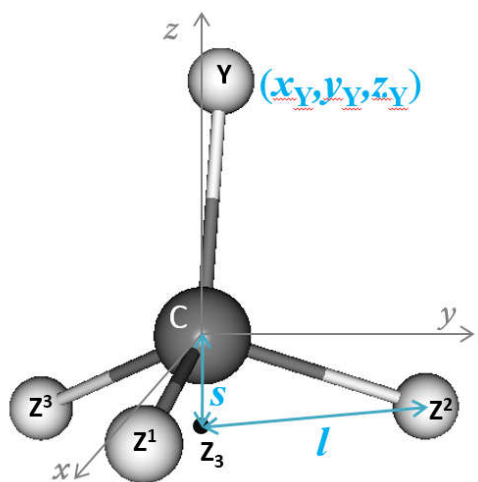


**Figure 2.** Opacity functions for reactions R1-R4 calculated at collision energy 1.36 eV on the (a) CBE and (b) ZBB3 PESs calculated with the RD and FD models. Per bond reaction probabilities are shown for easier comparison.

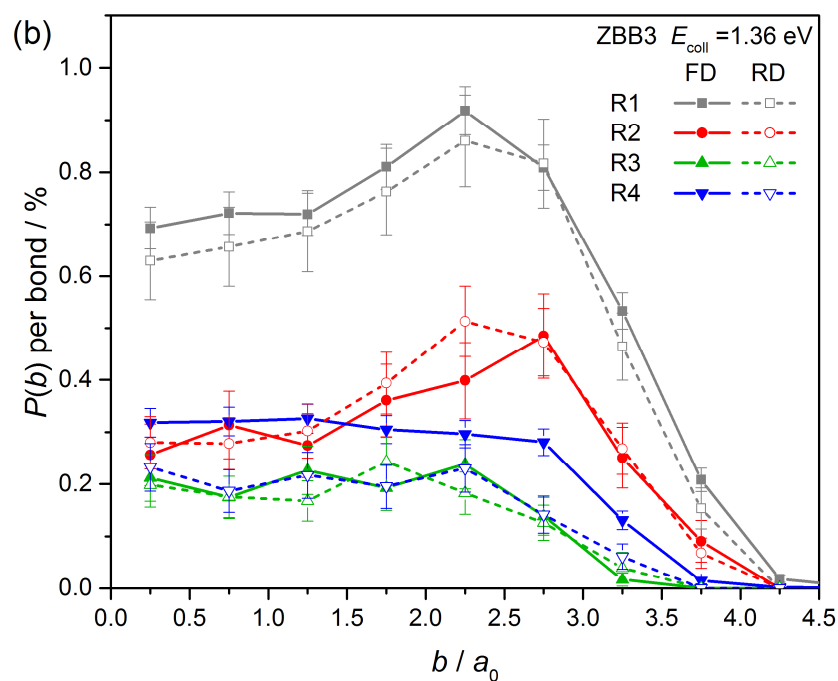
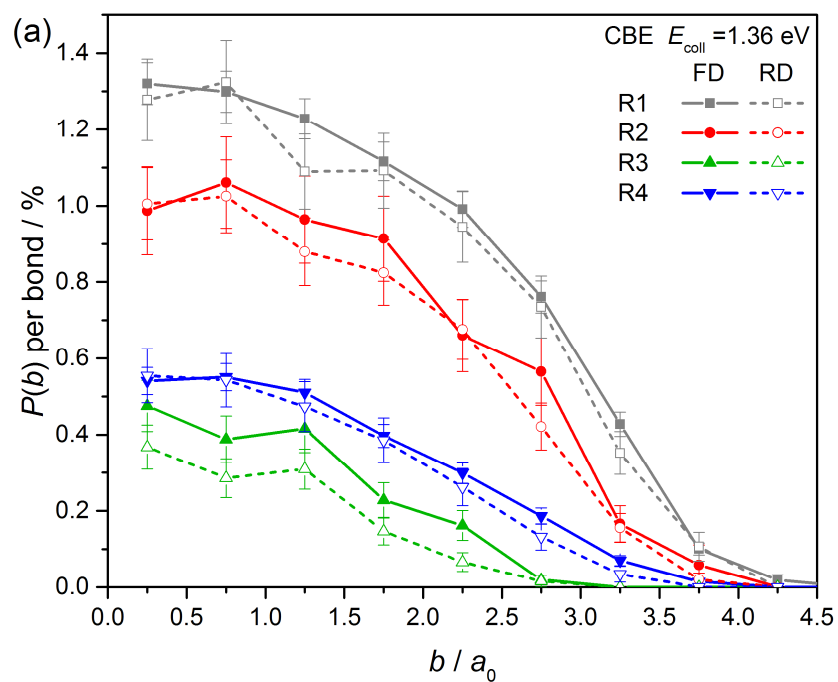


**Figure 3.** Excitation functions calculated for reactions R1 – R4 with the RD and FD models on the (a) CBE and (b) ZBB3 PESs. For easier comparison, per bond reaction cross sections are shown.

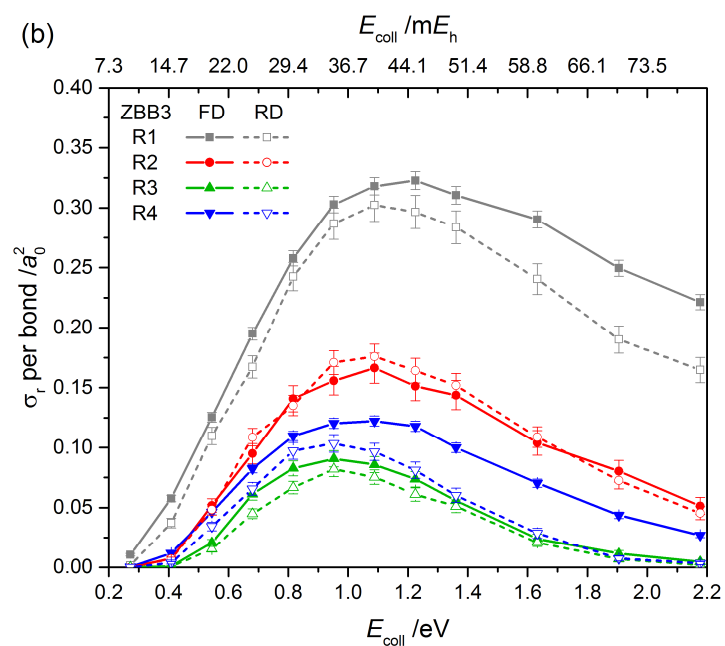
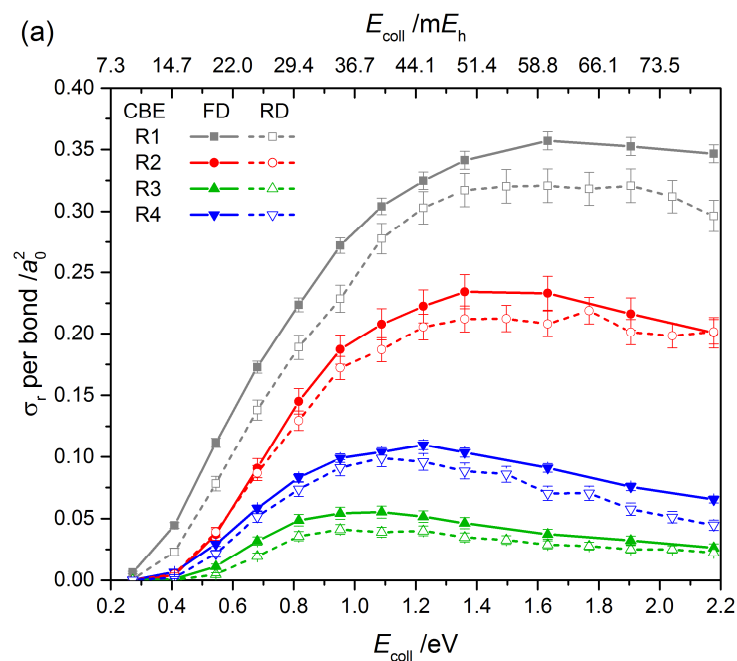


**Figure 4.** Product angular distributions calculated for reactions R1 – R4 with the RD and FD models on the (a) CBE and (b) ZBB3 PESs at  $E_{\text{coll}} = 1.36$  eV.

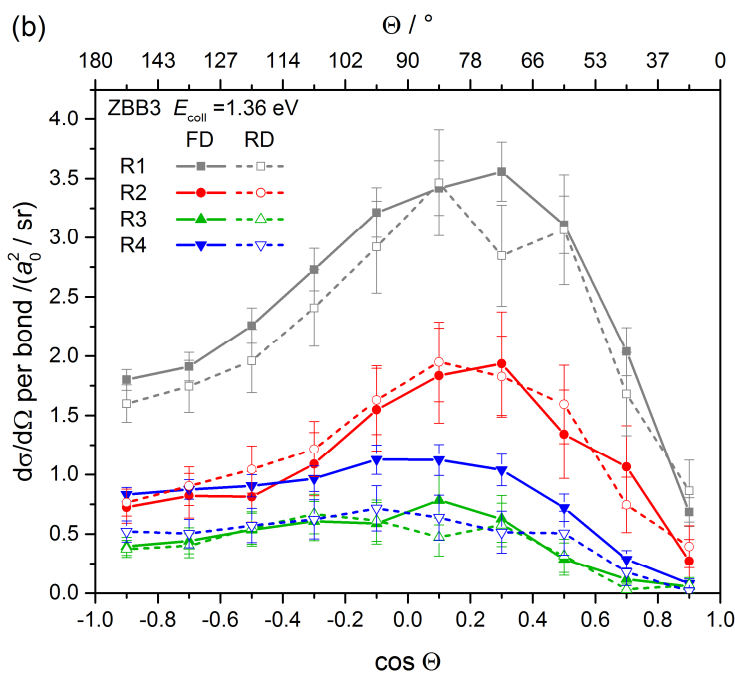
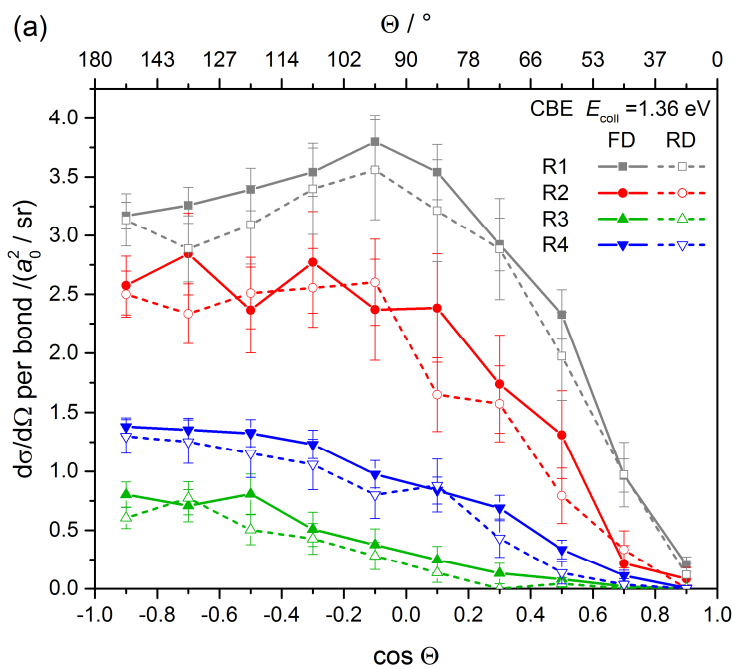
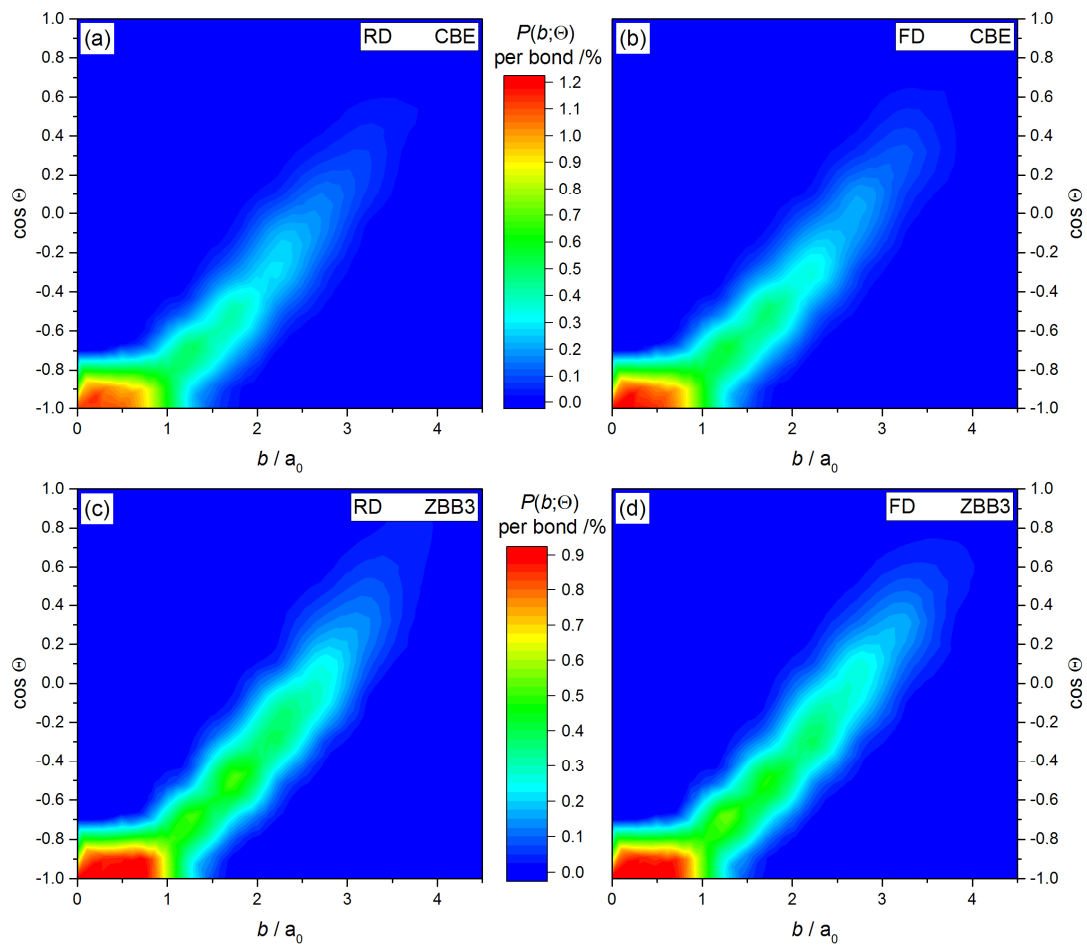


**Figure 5.** Scattering angle and impact parameter resolved reaction probabilities for reaction R1 calculated with the RD (a,c) and FD (b,d) models at collision energy 0.95 eV on the CBE (a,b) and ZBB3 (c,d) PESs. Per bond reaction probabilities are shown for easier comparison.

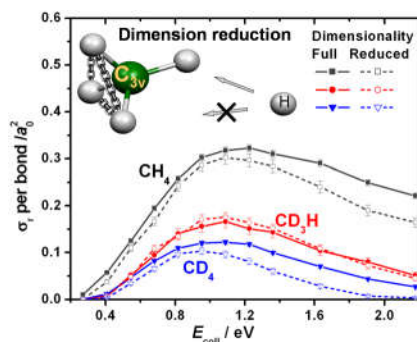


TABLES

Table 1. The irreducible representation, degeneracy and frequency of normal mode vibrations of the four methane isotopologs determined for the FD and 5D models on the CBE and ZBB3 PESs, and for comparison, the experimental frequencies.

Irrep.		Dege neracy		Type		Frequencies (cm <sup>-1</sup> )				
						CBE		ZBB3		Exp.
FD	5D	FD	5D	FD	5D	FD	5D	FD	5D	FD
<b>T<sub>d</sub></b>		<b>C<sub>3v</sub></b>		<b>CH<sub>4</sub></b>						
T <sub>2</sub>	A <sub>1</sub>	3	1	deg. deform.	CH <sub>3</sub> umbrella	1384	1384	1335	1335	1306
E	E	2	2	deg. deform.	CH <sub>3</sub> rock.	1551	1463	1548	1436	1534
A <sub>1</sub>	A <sub>1</sub>	1	1	sym. stre.	CH <sub>3</sub> sym. stre.	2994	2994	3026	3026	2917
T <sub>2</sub>	A <sub>1</sub>	3	1	deg. stre.	CH stre.	3167	3167	3167	3167	3019
<b>C<sub>3v</sub></b>		<b>C<sub>3v</sub></b>		<b>CD<sub>3</sub>H</b>						
A <sub>1</sub>	A <sub>1</sub>	1	1	CD <sub>3</sub> sym. deform.	CD <sub>3</sub> umbrella	1055	1055	1018	1018	1003
E	-	2	-	CD <sub>3</sub> deg. deform.	-	1070	-	1046	-	1036
E	E	2	2	CD <sub>3</sub> rock.	CD <sub>3</sub> rock.	1325	1323	1306	1299	1291
A <sub>1</sub>	A <sub>1</sub>	1	1	CD <sub>3</sub> sym. stre.	CD <sub>3</sub> sym. stre.	2168	2168	2187	2187	2142
E	-	2	-	CD <sub>3</sub> deg. stre.	-	2344	-	2344	-	2263
A <sub>1</sub>	A <sub>1</sub>	1	1	CH stre.	CH stre.	3130	3130	3137	3137	2993
<b>C<sub>3v</sub></b>		<b>C<sub>3v</sub></b>		<b>CH<sub>3</sub>D</b>						
E	E	2	2	CH <sub>3</sub> rock.	CH <sub>3</sub> rock.	1215	1241	1178	1219	1155
A <sub>1</sub>	A <sub>1</sub>	1	1	CH <sub>3</sub> sym. deform.	CH <sub>3</sub> umbrella	1379	1379	1330	1331	1300
E	-	2	-	CH <sub>3</sub> deg. deform.	-	1499	-	1488	-	1471
A <sub>1</sub>	A <sub>1</sub>	1	1	CD stre.	CD stre.	2279	2279	2287	2287	2200
A <sub>1</sub>	A <sub>1</sub>	1	1	CH <sub>3</sub> sym. stre.	CH <sub>3</sub> sym. stre.	3046	3046	3068	3068	2945
E	-	2	-	CH <sub>3</sub> deg. stre.	-	3167	-	3167	-	3017
<b>T<sub>d</sub></b>		<b>C<sub>3v</sub></b>		<b>CD<sub>4</sub></b>						
T <sub>2</sub>	A <sub>1</sub>	3	1	deg. deform.	CD <sub>3</sub> umbrella	1047	1047	1010	1010	996
E	E	2	2	deg. deform.	CD <sub>3</sub> rock.	1097	1071	1095	1052	1092
A <sub>1</sub>	A <sub>1</sub>	1	1	sym. stre.	CD <sub>3</sub> sym. stre.	2118	2118	2141	2141	2109
T <sub>2</sub>	A <sub>1</sub>	3	1	deg. stre.	CD stre.	2344	2344	2344	2344	2259

Table of Contents Graphic



## REFERENCES

- (1) Skouteris, D.; Castillo, J. F.; Manolopoulos, D. E. ABC: A Quantum Reactive Scattering Program. *Comput. Phys. Commun.* **2000**, *133*, 128–135.
- (2) Honvault, P.; Launay, J. M. Quantum Dynamics of Insertion Reactions. In *Theory of Chemical Reaction Dynamics*; Laganà, A.; Lendvay G., Eds.; NATO Sci. Ser.; Kluwer: Dordrecht, 2004, pp 187-215.
- (3) Rao, T. R.; Guillon, G.; Mahapatra, S.; Honvault, P. Huge Quantum Symmetry Effect in the O + O<sub>2</sub> Exchange Reaction. *J. Phys. Chem. Lett.* **2015**, *6*, 633–636.
- (4) Li, Y.; Sun, Z.; Jiang, B.; Xie, D.; Dawes, R.; Guo, H. Rigorous Quantum Dynamics of O + O<sub>2</sub> Exchange Reactions on an Ab Initio Potential Energy Surface Substantiate the Negative Temperature Dependence of Rate Coefficients. *J. Chem. Phys.* **2014**, *141*, 081102.
- (5) Pogrebnya, K.; Palma, J.; Clary D. C.; Echave, J. Quantum Scattering and Quasi-classical Trajectory Calculations for the H<sub>2</sub> + OH → H<sub>2</sub>O + H Reaction on a New Potential Surface. *Phys. Chem. Chem. Phys.*, **2000**, *2*, 693-700.
- (6) Fu, B.; Zhang, D.H. A Full-dimensional Quantum Dynamics Study of the Mode Specificity in the H + HOD Abstraction Reaction. *J. Chem. Phys.* **2015**, *142*, 064314.
- (7) Jiang, B.; Guo, H. Control of Mode/Bond Selectivity and Product Energy Disposal by the Transition State: X + H<sub>2</sub>O (X = H, F, O(<sup>3</sup>P), and Cl) Reactions. *J. Am. Chem. Soc.* **2013**, *135*, 15251–15256.
- (8) Schiffel, G.; Manthe, U. A Transition State View on Reactive Scattering: Initial State-selected Reaction Probabilities for the H + CH<sub>4</sub> → H<sub>2</sub> + CH<sub>3</sub> Reaction Studied in Full Dimensionality. *J. Chem. Phys.* **2010**, *133*, 174124.

- 
- (9) Welsch, R.; Manthe, U. Reaction Dynamics with the Multi-layer Multi-configurational Time-dependent Hartree Approach:  $\text{H} + \text{CH}_4 \rightarrow \text{H}_2 + \text{CH}_3$  Rate Constants for Different Potentials. *J. Chem. Phys.* **2012**, *137*, 244106.
- (10) Welsch, R.; Manthe, U. Full-dimensional and Reduced-dimensional Calculations of Initial State-selected Reaction Probabilities Studying the  $\text{H} + \text{CH}_4 \rightarrow \text{H}_2 + \text{CH}_3$  Reaction on a Neural Network PES. *J. Chem. Phys.* **2015**, *142*, 064309.
- (11) Truhlar, D.G.; Wyatt, R. E. The History of  $\text{H}_3$  Kinetics. *Annu. Rev. Phys. Chem.* **1976**, *27*, 1-43.
- (12) Kouri, D. J. In *Energy, Structure, and Reactivity*; Smith, D. W.; McRae, W. B., Eds.; Wiley: New York, 1973, p. 26.
- (13) George, T. F.; Ross, J. Quantum Dynamical Theory of Molecular Collisions. *Annu. Rev. Phys. Chem.* **1970**, *24*, 263-300.
- (14) Child, M. S. Measurable Consequences of a Dip in the Activation Barrier for an Adiabatic Chemical Reaction. *Mol. Phys.* **1967**, *12*, 401-416.
- (15) Connor, J. N. L.; Child, M. S. Differential Cross Sections for Chemically Reactive Systems. *Mol. Phys.* **1970**, *18*, 653-679.
- (16) Wyatt, R. E. Quantum Mechanics of the  $\text{H} + \text{H}_2$  Reaction: Investigation of Vibrational Adiabatic Models. *J. Chem. Phys.* **1969**, *51*, 3489-3502.
- (17) Walker, R. B.; Hayes, E. F. Reactive Scattering in the Bending-Corrected Rotating Linear Model. In *The Theory of Chemical Reaction Dynamics*; Clary, D. C., Ed.; Reidel: Dordrecht, 1986, pp 105-134.
- (18) Bowman, J. M. Reduced Dimensionality Theories of Quantum Reactive Scattering. *Adv. Chem. Phys.* **1986**, *61*, 115-167.
- (19) Clary, D. C. Quantum Reactive Scattering of Four-atom Reactions with Nonlinear Geometry:  $\text{OH} + \text{H}_2 \rightarrow \text{H}_2\text{O} + \text{H}$ . *J. Chem. Phys.* **1991**, *95*, 7298-7310.
- (20) Clary, D. C. Four-atom Reaction Dynamics, *J. Phys. Chem.* **1994**, *98*, 10678-10688.
- (21) Nyman, G.; Clary, D. C. Vibrational and Rotational Effects in the  $\text{Cl} + \text{HOD} \rightarrow \text{HCl} + \text{OD}$  Reaction. *J. Chem. Phys.* **1994**, *100*, 3556-3567.

- 
- (22) Bowman, J. M. Reduced Dimensionality Theory of Quantum Reactive Scattering. *J. Phys. Chem.* **1991**, *95*, 4960-4968.
- (23) Wang, D.; Bowman, J. M. Reduced Dimensionality Quantum Calculations of Mode Specificity in  $\text{OH} + \text{H}_2 \leftrightarrow \text{H}_2\text{O} + \text{H}$ . *J. Chem. Phys.* **1992**, *96*, 8906-8913.
- (24) Nyman, G.; Clary D. C. Quantum Scattering Calculations on the  $\text{CH}_4 + \text{OH} \rightarrow \text{CH}_3 + \text{H}_2\text{O}$  Reaction. *J. Chem. Phys.* **1994**, *101*, 5756-5771.
- (25) Nyman, G. 2D and 3D Quantum Scattering Calculations on the  $\text{CH}_4 + \text{OH} \rightarrow \text{CH}_3 + \text{H}_2\text{O}$  Reaction. *Chem. Phys. Letters* **1995**, *240*, 571-577.
- (26) Nyman, G. The Rotating Bond Umbrella Model Applied to Atom-methane Reactions. In *Theory of Chemical Reaction Dynamics*; Laganà, A.; Lendvay G., Eds.; NATO Sci. Ser., Kluwer: Dordrecht, 2004, pp 253-278.
- (27) Yu, H.-G.; Nyman, G. Three-dimensional Quantum Scattering Calculations on the  $\text{Cl} + \text{CH}_4 \rightarrow \text{HCl} + \text{CH}_3$  Reaction. *Phys. Chem. Chem. Phys.* **1999**, *1*, 1181-1190.
- (28) Yu, H.-G.; Nyman, G. Reaction Dynamics of Chlorine Atom with Methane: Dual-level Ab Initio Analytic Potential Energy Surface and Isotope effects. *J. Chem. Phys.* **1999**, *111*, 6693-6704.
- (29) Yu, H.-G.; Nyman, G. A Four Dimensional Quantum Scattering Study of the  $\text{Cl} + \text{CH}_4 \rightarrow \text{HCl} + \text{CH}_3$  Reaction via Spectral Transform Iteration. *J. Chem. Phys.* **1999**, *110*, 7233-7244.
- (30) Yu, H.-G.; Nyman, G. Quantum Dynamics of the  $\text{O}(^3\text{P}) + \text{CH}_4 \rightarrow \text{OH} + \text{CH}_3$  Reaction: An Application of the Rotating Bond Umbrella Model and Spectral Transform Subspace Iteration. *J. Chem. Phys.* **1999**, *110*, 7233-7244.
- (31) Zhang, J. Z. H. The Semirigid Vibrating Rotor Target Model for Quantum Polyatomic Reaction Dynamics. *J. Chem. Phys.* **1999**, *111*, 3929-3939.
- (32) Wang, M. L.; Li, Yimin; Zhang, J. Z. H.; Zhang, D. H. Application of Semirigid Vibrating Rotor Target Model to Reaction of  $\text{CH}_4 + \text{H} \rightarrow \text{CH}_3 + \text{H}_2$ . *J. Chem. Phys.* **2000**, *113*, 1802-1806.
- (33) Zhang, D. H.; Zhang, J. Z. H. The Semirigid Vibrating Rotor Target Model for Atom-polyatom Reaction: Application to  $\text{H} + \text{H}_2\text{O} \rightarrow \text{H}_2 + \text{OH}$ . *J. Chem. Phys.* **2000**, *112*, 585-591.

- 
- (34) Yang, M.; Zhang, J. Z. H. Stereodynamics and Rovibrational Effect for  $\text{H} + \text{CH}_4 (v,j,K,n) \rightarrow \text{H}_2 + \text{CH}_3$  Reaction. *J. Chem. Phys.* **2002**, *116*, 6497-6504.
- (35) Wang, M. L.; Zhang, J. Z. H. Generalized Semirigid Vibrating Rotor Target Model for Atom-polyatom Reaction: Inclusion of Umbrella Mode for the  $\text{H} + \text{CH}_4$  Reaction. *J. Chem. Phys.* **2002**, *117*, 3081-3087.
- (36) Wang, D.; Bowman, J. M. A Reduced Dimensionality, Six-degree-of-freedom, Quantum Calculation of the  $\text{CH}_4 + \text{H} \rightarrow \text{CH}_3 + \text{H}_2$  Reaction. *J. Chem. Phys.* **2001**, *115*, 2055-2061.
- (37) Palma, J.; Clary, D. C. A Quantum Model Hamiltonian to Treat Reactions of the Type  $\text{X} + \text{Y}\text{CZ}_3 \rightarrow \text{XY} + \text{CZ}_3$ . Application to  $\text{O}(^3\text{P}) + \text{CH}_4 \rightarrow \text{OH} + \text{CH}_3$ . *J. Chem. Phys.* **2000**, *112*, 1859-1867.
- (38) Palma, J.; Clary, D. C. Improving Reduced Dimensionality Quantum Reaction Dynamics with a Generalized Transition State. Application to  $\text{O}(^3\text{P}) + \text{CH}_4 \rightarrow \text{OH} + \text{CH}_3$ . *J. Chem. Phys.* **2000**, *115*, 2188-2197.
- (39) Palma, J.; Echave, J.; Clary D. C. Rate Constants for the  $\text{CH}_4 + \text{H} \rightarrow \text{CH}_3 + \text{H}_2$  Reaction Calculated with a Generalized Reduced-Dimensionality Method. *J. Phys. Chem. A* **2002**, *106*, 8256-8260.
- (40) Zhang, D. H., Yang, M., Collins, M. A., Lee, S.-Y., Reaction Dynamics of Polyatomic Systems: from  $\text{A} + \text{BCD}$  to  $\text{X} + \text{Y}\text{CZ}_3$ . In *Theory of Chemical Reaction Dynamics*; Laganà, A.; Lendvay G., Eds.; NATO Sci. Ser.; Kluwer: Dordrecht, 2004, pp 279-303.
- (41) Yang, M. H.; Zhang, D. H.; Lee, S.-Y. A Seven-dimensional Quantum Study of the  $\text{H} + \text{CH}_4$  Reaction. *J. Chem. Phys.* **2002**, *117*, 9539-9542.
- (42) Yang, M. H.; Zhang, D. H.; Lee, S.-Y. Seven-dimensional Quantum Dynamics Study of the  $\text{O}(^3\text{P}) + \text{CH}_4$  Reaction. *J. Chem. Phys.* **2007**, *126*, 064303.
- (43) Zhou, Y.; Fu, B.; Wang, C. R.; Collins, M. A.; Zhang, D. H. Ab Initio Potential Energy Surface and Quantum Dynamics for the  $\text{H} + \text{CH}_4 \rightarrow \text{H}_2 + \text{CH}_3$  Reaction. *J. Chem. Phys.* **2011**, *134*, 064323.
- (44) Wang, Y.; Li, J.; Guo, H.; Yang, M. H. A Comparison Study of the  $\text{H} + \text{CH}_4$  and  $\text{H} + \text{SiH}_4$  Reactions with Eight-Dimensional Quantum Dynamics: Normal Mode Versus Local Mode in the Reactant Molecule Vibration. *Theor. Chem. Acc.* **2014**, *133*, 1555.
- (45) Liu, N.; Zhang, M. H. An Eight-dimensional Quantum Dynamics Study of the  $\text{Cl} + \text{CH}_4 \rightarrow \text{HCl} + \text{CH}_3$  Reaction. *J. Chem. Phys.* **2015**, *143*, 134305.

- 
- (46) Kerkeni, B.; Clary D. C. Ab Initio Rate Constants from Hyperspherical Quantum Scattering: Application to  $\text{H} + \text{CH}_4 \rightarrow \text{H}_2 + \text{CH}_3$ . *J. Chem. Phys.* **2004**, *120*, 2308-2318.
- (47) Bowman, J. M.; Wagner, A. F. Reduced Dimensionality Theories of Quantum Reactive Scattering: Applications to  $\text{Mu} + \text{H}_2$ ,  $\text{H} + \text{H}_2$ ,  $\text{O}(^3\text{P}) + \text{H}_2$ ,  $\text{D}_2$  and  $\text{HD}$ . In *The Theory of Chemical Reaction Dynamics*; Clary, D. C., Ed.; Reidel: Dordrecht, 1986, pp 47-76.
- (48) Bowman, J. M.; Ju, G.-Z.; Lee, K. T.; Wagner A. F.; Schatz, G. C. Tests of collinear Quasiclassical Trajectory Transmission Coefficient Correction to Transition State Theory. *J. Chem. Phys.* **1981**, *75*, 141-147.
- (49) Kerkeni B.; Clary, D. C. The Effect of the Torsional and Stretching Vibrations of  $\text{C}_2\text{H}_6$  on the  $\text{H} + \text{C}_2\text{H}_6 \rightarrow \text{H}_2 + \text{C}_2\text{H}_5$  Reaction. *J. Chem. Phys.* **2005**, *123*, 064305.
- (50) Kerkeni B.; Clary, D. C. Quantum Reactive Scattering of  $\text{H} + \text{Hydrocarbon}$  Reactions. *Phys. Chem. Chem. Phys.* **2006**, *8*, 917-925.
- (51) Clary, D. C.; Meijer, A. J. M. Excitation of Torsional Modes of Proteins via Collisional Energy Transfer: A Quantum Dynamical Approach, *J. Chem. Phys.* **2002**, *116*, 9829-9838.
- (52) Zhang, W.; Zhou, Y.; Wu G.; Lu, Y.; Pana H.; Fu, B.; Shuai, Q.; Liu, L.; Liu, S.; Zhang, L.; et al. Depression of Reactivity by the Collision Energy in the Single Barrier  $\text{H} + \text{CD}_4 \rightarrow \text{HD} + \text{CD}_3$  Reaction. *Proc. Natl. Acad. Sci. U.S.A.* **2010**, *107*, 12782-12785.
- (53) Corchado, J. C.; Bravo, J. L.; Espinosa-Garcia, J. The Hydrogen Abstraction Reaction  $\text{H} + \text{CH}_4$ . I. New Analytical Potential Energy Surface Based on Fitting to Ab Initio Calculations. *J. Chem. Phys.* **2009**, *130*, 184314.
- (54) Zhang, X.; Braams, B. J.; Bowman, J. M. An Ab Initio Potential Surface Describing Abstraction and Exchange for  $\text{H} + \text{CH}_4$ . *J. Chem. Phys.* **2006**, *124*, 021104.
- (55) Raff, L. M.; Thompson, D.L. The Classical Trajectory Approach to Reactive Scattering. In *Theory of Chemical Reaction Dynamics*; Baer, M., Ed.; CRC Press: Boca Raton, 1985, Vol. 3, pp 1-123.
- (56) Nagy, T.; Vikár, A.; Lendvay, G. Oscillatory Reaction Cross Sections Caused by Normal Mode Sampling in Quasiclassical Trajectory Calculations. *J. Chem. Phys.* **2016**, *144*, 014104.

- 
- (57) Sloane, C. S.; Hase, W. L. On the Dynamics of State Selected Unimolecular Reactions: Chloroacetylene Dissociation and Predissociation. *J. Chem. Phys.* **1977**, *66*, 1523-1533.
- (58) Mátyus, E.; Czakó, G.; Császár, A. G. Toward Black-box-type Full- and Reduced-Dimensional Variational (Ro)Vibrational Computations. *J. Chem. Phys.* **2009**, *130*, 134112.
- (59) Marsaglia, G.; Zaman, A. A New Class of Random Number Generators. *Annals of Applied Probability*, **1991**, *1*, 462-480.
- (60) Chandler, R.; Northrop, P. <http://www.ucl.ac.uk/~ucajarc/work/randgen.html>, version 26/08/2003. Accessed Jan. 05, 2016.
- (61) Espinosa-Garcia, J. New Analytical Potential Energy Surface for the CH<sub>4</sub> + H Hydrogen Abstraction Reaction: Thermal Rate Constants and Kinetic Isotope Effects. *J. Chem. Phys.* **2002**, *116*, 10664-10673.
- (62) Camden, J. P.; Hu, W.; Bechtel, H. A.; Brown, D. J. A.; Martin, M. R.; Zare, R. N.; Lendvay, G.; Troya, D.; Schatz, G. C. H + CD<sub>4</sub> Abstraction Reaction Dynamics: Excitation Function and Angular Distributions. *J. Phys. Chem. A* **2006**, *110*, 677-686.
- (63) Hu, W.; Lendvay, G.; Troya, D.; Schatz, G. C.; Camden, J. P.; Bechtel, H. A.; Brown, D. J. A.; Martin, M. R.; Zare, R. N. H + CD<sub>4</sub> Abstraction Reaction Dynamics: Product Energy Partitioning. *J. Phys. Chem. A* **2006**, *110*, 3017-3027..
- (64) Camden, J. P.; Bechtel, H. A.; Brown, D. J. A.; Martin, M. R.; Zare, R. N.; Hu, W.; Lendvay, G.; Troya, D.; Schatz, G. C. A Reinterpretation of the Mechanism of the Simplest Reaction at an sp<sup>3</sup>-Hybridized Carbon Atom: H + CD<sub>4</sub> → CD<sub>3</sub> + HD. *J. Am. Chem. Soc.* **2005**, *127*, 11898-11899.
- (65) Szabó, P.; Lendvay, G. A Quasiclassical Trajectory Study of the Reaction of H Atoms with O<sub>2</sub>(<sup>1</sup>Δ<sub>g</sub>). *J. Phys. Chem. A* **2015**, *119*, 7180-7189.
- (66) Szabó, P.; Lendvay, G. Dynamics of Complex-Forming Bimolecular Reactions: A Comparative Theoretical Study of the Reactions of H Atoms with O<sub>2</sub>(<sup>3</sup>Σ<sub>g</sub><sup>-</sup>) and O<sub>2</sub>(<sup>1</sup>Δ<sub>g</sub>). *J. Phys. Chem. A* **2015**, *119*, 12485–12497.

(67) Lahankar, S.A.; Zhang, J.; Minton, T.K.; Guo, H.; Lendvay, G. Dynamics of the O-Atom Exchange Reaction  $^{16}\text{O}(^3\text{P}) + ^{18}\text{O}^{18}\text{O}(^3\Sigma_g^-) \rightarrow ^{16}\text{O}^{18}\text{O}(^3\Sigma_g^-) + ^{18}\text{O}(^3\text{P})$  at Hyperthermal Energies, *J. Phys. Chem. A*, submitted.

## TOC Graphics

